Theor. Comput. Fluid Dyn. (2017) 31:51–66
DOI 10.1007/s00162-016-0401-1

ORIGINAL ARTICLE

Andrew D. Bragg · Susan Kurien · Timothy T. Clark

Model of non-stationary, inhomogeneous turbulence

Received: 8 December 2015 / Accepted: 21 June 2016 / Published online: 8 July 2016

Abstract We compare results from a spectral model for non-stationary, inhomogeneous turbulence (Besnard et al. in Theor Comp Fluid Dyn 8:1–35, 1996) with direct numerical simulation (DNS) data of a shear-free mixing layer (SFML) (Tordella et al. in Phys Rev E 77:016309, 2008). The SFML is used as a test case in which the efficacy of the model closure for the physical-space transport of the fluid velocity field can be tested in a flow with inhomogeneity, without the additional complexity of mean-flow coupling. The model is able to capture certain features of the SFML quite well for intermediate to long times, including the evolution of the mixing-layer width and turbulent kinetic energy. At short-times, and for more sensitive statistics such as the generation of the velocity field anisotropy, the model is less accurate. We propose two possible causes for the discrepancies. The first is the local approximation to the pressure-transport and the second is the a priori spherical averaging used to reduce the dimensionality of the solution space of the model, from wavevector to wavenumber space. DNS data are then used to gauge the relative importance of both possible deficiencies in the model.

Keywords Turbulence modeling · Inhomogeneous turbulence · Two-point modeling · Turbulent mixing · Non-stationary turbulence

1 Introduction

Developing theoretical models that can predict the statistical features of inhomogeneous, turbulent flows presents a major challenge, and there are several possible approaches and perspectives to consider. One important choice is to determine the space in which one wishes to describe the turbulence statistics, e.g. a 'one-point' space (describing the turbulent statistics at one point in space $\boldsymbol{x}$) or a 'multi-point' space (describing the turbulent statistics at multiple, distinct points in space $\boldsymbol{x}_1, \boldsymbol{x}_2 ... \boldsymbol{x}_n$). This choice is largely determined by the desired balance between the solvability of the model and the level of faithfulness one wishes to retain to the true turbulent dynamics. The majority of modeling efforts have tended to focus on one-point models, often in the context of the so-called 'Two Equation Models' (see Pope [1]). However, from a fundamental perspective, the models should at least describe the turbulence at the two-point level. This is both because the incompressible Navier–Stokes equation (NSE) is itself *essentially* a two-point system, since the pressure field is non-local in

Communicated by Dr. Philippe Spalart.

Andrew D. Bragg (✉) · Susan Kurien
Applied Mathematics and Plasma Physics Group, Los Alamos National Laboratory, Los Alamos, NM 87545, USA
E-mail: adbragg265@gmail.com

Timothy T. Clark
Department of Mechanical Engineering, University of New Mexico, Albuquerque, NM, USA

physical space, and also because processes such as the energy transfer among the scales of motion in turbulence cannot, by definition, be described with less than two-points since a single point carries no information on scale.

The motivation for two-point models arises not only from fundamental, but also practical considerations. In particular, one-point models utilize a single scale, associated with the most energetic scales of the turbulence, to construct closure expressions for transport equations. The use of a single-scale closure implicitly assumes that the distribution of energy among the scales of motion is in a state of statistical equilibrium (see [2–5]), and as such, one-point models are intrinsically unsuitable for describing flows undergoing strong transients. This is not to say that one-point models could not be "tuned" to match the results of such flows, but it is to say that the resulting agreement would arise for the wrong reasons.

In light of such considerations, Besnard et al. [6] (referred to hereafter as BHRZ) developed a two-point model for describing turbulent flows that are strongly out of statistical equilibrium. Their aim was to develop a model that captured the physical process necessary for predicting such flows, but that was also as simple as possible so as to be useful for practical calculations. Therefore, instead of using more formal approaches such as renormalized perturbation theory (e.g. [7–10]), they used a phenomenological approach in which the non-linear and non-local processes of the turbulence are represented by simple terms in the equations that reproduce the correct, known qualitative behavior. The modeling philosophy behind the BHRZ model is similar in spirit to some of the earlier models such as that of Daly and Harlow [11] and that of Launder et al. [12], but extrapolates the modeling ideas in these works to the two-point space. The BHRZ model can be reduced to a one-point model, i.e., a Reynolds stress–Epsilon model, via constructing the spectral-space moments of the equations [5]. However, the resultant one-point model suffers from the limitations inherent in such models, i.e., the inability to accurately model flows undergoing strong transients.

A drawback with two-point models is, of course, the additional computational effort required to solve their equations compared with one-point models. However, with modern computing power, solving two-point models is more than feasible, to the extent that it is no longer necessary to invoke all of the additional assumptions so as to construct simpler one-point models.

Previous comparisons of the BHRZ model with homogeneous sheared and strained turbulence in Clark and Zemach [13] showed good agreement, and that the model was able to capture certain non-trivial aspects of the flow. Detailed investigations of the validity of the BHRZ model for predicting non-stationary, inhomogeneous turbulent flows have not, however, been undertaken, and this is precisely the purpose of the present paper. It is the way that the BHRZ models the physical-space transport of the turbulent velocity fluctuations that is of primary concern, since the model made several approximations in describing this processes. The closure model employed in BHRZ for the physical-space transport also contains an unknown constant; one of the aims of the present work is to obtain an estimate for this constant.

We compare the BHRZ model with DNS data from a Shear-Free Mixing Layer (SFML). In the SFML the turbulent kinetic energy propagates from a region of strong turbulence into a region of weak turbulence through a mixing process driven solely by the inhomogeneity (the SFML is explained in detail in Sect. 2). Such flows have also been studied in the laboratory [14,15] and provide useful paradigms for understanding turbulent mixing processes in isolation from more complex mean-flow coupled processes. Indeed, the main reason for this choice of test case for our study is that it allows us to test the BHRZ closure model used for the physical-space transport of the turbulent velocity fluctuations independently of mean-flow coupled terms which would add additional modeling complications.

The outline of the paper is as follows: In Sect. 2 we explain the SFML, the physical mechanisms that govern its evolution, and the particular statistical features of the flow. Next, in Sect. 3 we introduce the BHRZ model and discuss in detail the various approximations made in its derivation. We also discuss the initial and boundary conditions used in the model for the SFML. In Sect. 4 we compare the predictions from the BHRZ model with direct numerical simulation (DNS) data of a SFML. Finally, in Sect. 5 we draw conclusions to the work and identify features of the BHRZ model that need to be improved in future work in order for it to more accurately predict strongly non-stationary, inhomogeneous and anisotropic turbulent flows.

2 Shear-free mixing layer

In this section we first describe the SFML simulated in Tordella et al. [16], against which we shall compare the BHRZ model predictions in Sect. 4, and then consider the physical mechanisms governing its evolution and the statistical characteristics of the flow.

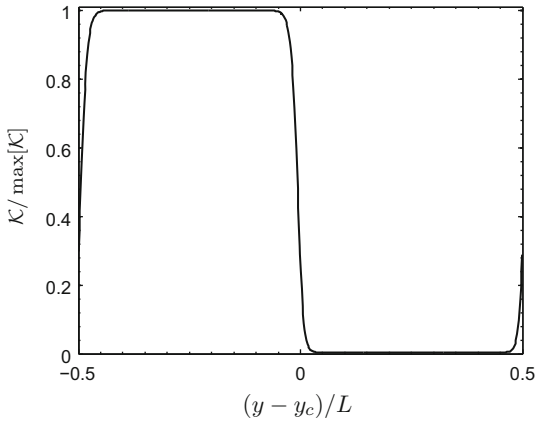

Fig. 1 Illustration of the turbulent kinetic energy, $\mathcal{K}(y,t)$, in a SFML, where $y \in [0, L]$, L is the periodic lengthscale of $\mathcal{K}(y,t)$ and $y_c \equiv L/2$

Figure 1 illustrates the turbulent kinetic energy (TKE), $\mathcal{K}(y,t)$, in the SFML. The function satisfies $\mathcal{K}(y,t) = \mathcal{K}(y+L,t)$ where $y \in [0, L]$ and L is the periodic lengthscale. At $t = 0$ the ratio of the maximum to the minimum TKE in the SFML is given by $\gamma \equiv \max[\mathcal{K}(y,0)]/\min[\mathcal{K}(y,0)]$, and by varying γ, the strength of the initial inhomogeneity in the SFML can be controlled, and its effect upon the resulting flow can be examined. Note that in Tordella et al. [16], only the TKE is inhomogeneous in the initial flow field; the integral lengthscale is homogeneous.

In Tordella et al. [16], the initial velocity field for the SFML is constructed as follows: Let $\boldsymbol{u}^{[1]}(\boldsymbol{x},t)$ be an incompressible Navier–Stokes turbulent velocity field that is statistically stationary, homogeneous and isotropic. Now define a second velocity field $\boldsymbol{u}^{[2]}(\boldsymbol{x},t) \equiv \lambda \boldsymbol{u}^{[1]}(\boldsymbol{x},t)$, where λ is a constant ≤ 1. The initial velocity field for the SFML is then constructed as

$$\boldsymbol{u}(\boldsymbol{x},0) \equiv P(y)\boldsymbol{u}^{[1]}(\boldsymbol{x},0) + \Big(1 - P(y)\Big)\boldsymbol{u}^{[2]}(\boldsymbol{x},0), \tag{1}$$

where $y \equiv x_2$ is the inhomogeneous, mixing direction. The function $P(y) \in [0, 1]$, such that in the 'low energy region', $\boldsymbol{u}^{[2]}(\boldsymbol{x},0)$ describes the initial velocity field, and in the 'high energy region', $\boldsymbol{u}^{[1]}(\boldsymbol{x},0)$ describes the initial velocity field, and satisfies $P(y) = P(y+L)$. The particular form of $P(y)$ used in Tordella et al. [16] is

$$P(y) = \frac{1}{2}\Big(1 + \tanh\Big[ay/L\Big]\tanh\Big[a(y - L/2)/L\Big]\tanh\Big[a(y - L)/L\Big]\Big), \tag{2}$$

with $a = 20\pi$ and $L = 4\pi$.

Due to the presence of $P(y)$, (1) generates $\boldsymbol{\nabla}\cdot\boldsymbol{u}(\boldsymbol{x},0) \neq \boldsymbol{0}$. In order to generate an initial field that is incompressible, (1) is projected onto a divergence-free field, and then λ is rescaled so that the resulting incompressible velocity field possesses the desired value of γ. By repeating this procedure iteratively, one obtains an initial velocity field that is incompressible with γ arbitrarily close to the desired value.

$$\begin{aligned}\Big\langle \boldsymbol{u}(\boldsymbol{x},0)\boldsymbol{u}(\boldsymbol{x},0)\Big\rangle \equiv\ & P^2\Big\langle \boldsymbol{u}^{[1]}(\boldsymbol{x},0)\boldsymbol{u}^{[1]}(\boldsymbol{x},0)\Big\rangle + P\Big(1-P\Big)\Big\langle \boldsymbol{u}^{[1]}(\boldsymbol{x},0)\boldsymbol{u}^{[2]}(\boldsymbol{x},0)\Big\rangle \\ & + P\Big(1-P\Big)\Big\langle \boldsymbol{u}^{[2]}(\boldsymbol{x},0)\boldsymbol{u}^{[1]}(\boldsymbol{x},0)\Big\rangle + \Big(1-P\Big)^2\Big\langle \boldsymbol{u}^{[2]}(\boldsymbol{x},0)\boldsymbol{u}^{[2]}(\boldsymbol{x},0)\Big\rangle, \end{aligned} \tag{3}$$

$$\Big\langle \boldsymbol{u}(y,0)\boldsymbol{u}(y,0)\Big\rangle = (2/3)\mathcal{K}^{[1]}\Big(P^2 + \gamma[1-P]\Big(2P + \gamma[1-P]\Big)\Big)\mathbf{I}, \tag{4}$$

$$\mathcal{K}(y,0) = \mathcal{K}^{[1]}\Big(P^2 + \gamma[1-P]\Big(2P + \gamma[1-P]\Big)\Big), \tag{5}$$

The resulting initial velocity field $\boldsymbol{u}(\boldsymbol{x},0)$ constructed in this manner then has the properties $\langle \boldsymbol{u}(y,0)\boldsymbol{u}(y,0)\rangle = \langle \boldsymbol{u}(y+L,0)\boldsymbol{u}(y+L,0)\rangle$ and $\langle \boldsymbol{u}(y,0)\boldsymbol{u}(y,0)\rangle \propto \mathbf{I}$, where $\mathbf{I}$ is the identity tensor. The parameter γ will be used as a control parameter in Sect. 4 to vary the strength of the initial inhomogeneity of the SFML.

Having defined the construction of $\boldsymbol{u}(\boldsymbol{x},0)$, and hence $\mathcal{K}(y,0)$, we now consider how $\mathcal{K}(y,t)$ evolves as the flow mixes. The initial flow is inhomogeneous in the y direction, and consequently the transport mechanisms

in the flow proceed to mix the TKE. The flow remains homogeneous in the (x_1, x_2) directions, such that the flow exhibits cylindrical symmetry about the $y \equiv x_2$ axis. In Tordella et al. [16] this fact is exploited for the construction of the statistics of the flow field which are constructed as averages over the (x_1, x_2)-plane, for a given y, t. The transport equation governing $\mathcal{K}(y,t)$ in the SFML is given by

$$\partial_t \mathcal{K}(y,t) = \underbrace{-(1/2)\partial_y \mathrm{tr}[\langle \boldsymbol{u}\boldsymbol{u}u_2\rangle]}_{\text{Self-transport}} \underbrace{-(1/2)\partial_y\langle u_2 p\rangle}_{\text{Pressure-transport}} + \underbrace{(\nu/2)\partial_y^2\mathcal{K}}_{\text{Molecular transport}} \underbrace{-\nu\langle \boldsymbol{\partial_x u} : \boldsymbol{\partial_x u}\rangle}_{\text{Dissipation}}, \tag{6}$$

where $\mathcal{K}(y,t) \equiv (1/2)\mathrm{tr}[\langle \boldsymbol{u}(y,t)\boldsymbol{u}(y,t)\rangle]$, $\boldsymbol{u}(\boldsymbol{x},t)$ is the fluid velocity field, $p(\boldsymbol{x},t)$ is the pressure field, and ν is the kinematic viscosity of the fluid. Note that in the SFML that we are considering, $\langle \boldsymbol{u}(\boldsymbol{x},t)\rangle = \boldsymbol{0}\,\forall t$ and therefore $\boldsymbol{u}(\boldsymbol{x},t)$ represents the fluctuating velocity field.

When $\boldsymbol{u}(\boldsymbol{x},t)$ is turbulent, the contribution from the self-transport and pressure-transport terms will typically dominate the overall transport of $\mathcal{K}$ in physical space, with molecular diffusion transport playing a small role. For the SFML that we are considering, the initial velocity field satisfies $\langle \boldsymbol{u}(y,0)\boldsymbol{u}(y,0)\rangle \propto \mathbf{I}$. With this initial condition, it is straightforward to show that the self-transport and pressure-transport terms in the equation governing the evolution of $\langle \boldsymbol{u}(y,t)\boldsymbol{u}(y,t)\rangle$ are the only terms that are able to generate pointwise anisotropy in the flow field. It is this, combined with the dominance of the self-transport and pressure-transport terms in the mixing process, that makes the SFML a good test case for the BHRZ model since it provides a flow configuration for which the BHRZ closure modeling for the physical-space transport of $\boldsymbol{u}(\boldsymbol{x},t)$ can be scrutinized.

One of the significant complexities of inhomogeneous turbulent flows is that the physical-space transport is non-local because of the contribution from the pressure field. Although the pressure field is dynamically non-local in any turbulent flow, it only makes an explicit, finite statistical contribution to the evolution of $\mathcal{K}(y,t)$ when the flow is inhomogeneous. This may be seen by noting that for an incompressible turbulent flow, $(\boldsymbol{\partial_x}\cdot\boldsymbol{\partial_x})p(\boldsymbol{x},t) = -\,\boldsymbol{\partial_x}\boldsymbol{\partial_x} : [\boldsymbol{u}(\boldsymbol{x},t)\boldsymbol{u}(\boldsymbol{x},t)]$, and by expressing the solution to this Poisson equation using a Green function, G, we may write

$$\boldsymbol{\partial_x}\langle \boldsymbol{u}(\boldsymbol{x},t)p(\boldsymbol{x},t)\rangle = -\boldsymbol{\partial_x}\int_{\mathbb{R}^3} G(\boldsymbol{x},\boldsymbol{x}')\;\boldsymbol{\partial_{x'}}\boldsymbol{\partial_{x'}} : \Big\langle \boldsymbol{u}(\boldsymbol{x},t)\boldsymbol{u}(\boldsymbol{x}',t)\boldsymbol{u}(\boldsymbol{x}',t)\Big\rangle d\boldsymbol{x}'. \tag{7}$$

The complexity that this non-locality introduces is problematic both computationally, since it renders the evolution equation for $\mathcal{K}(y,t)$ of integro-differential form, and also theoretically, because it requires knowledge of the two-point statistic $\langle u_2(y,t)u_2(y',t)u_2(y',t)\rangle$. In contrast to turbulent flows with a mean velocity field, in Tordella et al. [16] it was observed that for the SFML, the self-transport does not dominate the pressure-transport. Consequently, in constructing models for the SFML, errors incurred by making approximations to the pressure-transport (such as a local approximation) could have a significant effect on the overall predictions of the model for the SFML. We will return to this topic throughout the paper, in considering how the BHRZ model closes the pressure-transport contribution and also in considering the effects of the closure model on the ability of BHRZ to accurately describe inhomogeneous flows.

We now turn to consider some of the statistical features of the SFML during its evolution. The initial inhomogeneity of $\mathcal{K}$ leads to a mixing of the TKE of the flow through the action of the transport mechanisms described by (6), and these transport mechanisms drive the velocity field toward the asymptotically homogeneous state $\lim_{t\to\infty}(\max[\mathcal{K}(y,t)]/\min[\mathcal{K}(y,t)]) \to 1$. The results in Tordella et al. [16] showed that after a time period of $t/\tau \approx 3$, where τ is the integral timescale of the initial field $\boldsymbol{u}^{[1]}(\boldsymbol{x},t)$, the SFML enters a self-similar regime, during which the statistics of $\boldsymbol{u}(\boldsymbol{x},t)$ become approximately constant when normalized in appropriate ways. The self-similar regime corresponds to the regime where the competition between the physical mechanisms governing the evolution have come to a sort of 'equilibrium'. For example, in the self-similar regime, the flow field anisotropy is approximately constant, indicating that the transport mechanisms generating the anisotropy have reached an equilibrium state where they balance out the return to isotropy processes acting in the field. It is in fact only the transport mechanisms that can break the pointwise isotropic symmetry of the initial field $\boldsymbol{u}(\boldsymbol{x},0)$ as the mixing occurs, since there is no mean-shear in the SFML. The transport terms break the isotropic symmetry of the velocity field because different components of the velocity field are transported at different rates. For example, the self-transport is $-\partial_y\langle \boldsymbol{u}(y,t)\boldsymbol{u}(y,t)u_2(y,t)\rangle$ and its contribution to $\partial_t\langle u_1(y,t)u_1(y,t)\rangle$ and $\partial_t\langle u_2(y,t)u_2(y,t)\rangle$ will differ since $\langle u_1(y,t)u_1(y,t)u_2(y,t)\rangle \neq \langle u_2(y,t)u_2(y,t)u_2(y,t)\rangle$ (since u_2 is more correlated with itself than with u_1).

In an early experimental study on the SFML, Gilbert [17] found that the Probability Density Function (PDF) of $\boldsymbol{u}(\boldsymbol{x},t)$ remained essentially Gaussian throughout the evolution of the mixing process. In subsequent

experiments on the SFML performed by Veeravalli and Warhaft [14], a very different behavior was observed, with $\boldsymbol{u}(\boldsymbol{x},t)$ exhibiting strong departures from Gaussianity. Veeravalli and Warhaft attributed this to the fact that in Gilbert's experiments, $\max[\mathcal{K}(y,0)]/\min[\mathcal{K}(y,0)]$ was too low ($\approx$1.48) for the transport mechanisms to substantially drive the PDF of $\boldsymbol{u}(\boldsymbol{x},t)$ away from its initial Gaussian form. In both Gilbert's and Veeravalli and Warhaft's experiments on the SFML, there was an inhomogeneity in both the initial TKE and the initial integral lengthscale across the mixing layer.

The purpose of the study in Tordella et al. [16] was to demonstrate that an inhomogeneity in the initial TKE alone is a sufficient condition for the PDF of $\boldsymbol{u}(\boldsymbol{x},t)$ to deviate from its Gaussian form at $t=0$. They observed strong departures from Gaussianity, and that the field became more non-Gaussian with increasing $\max[\mathcal{K}(y,0)]/\min[\mathcal{K}(y,0)]$, until the field reached a saturation point at $\max[\mathcal{K}(y,0)]/\min[\mathcal{K}(y,0)] = \mathcal{O}(100)$ above which the non-Gaussianity did not continue to grow. The maximum skewness of $\boldsymbol{u}(\boldsymbol{x},t)$ in the mixing layer reached an approximately constant value of 1 at long times for $\max[\mathcal{K}(y,0)]/\min[\mathcal{K}(y,0)] = 12$, and reached an approximately constant value of 2.25 at long times for $\max[\mathcal{K}(y,0)]/\min[\mathcal{K}(y,0)] = 300$. The maximum kurtosis of $\boldsymbol{u}(\boldsymbol{x},t)$ in the mixing layer reached an approximately constant value of 4 at long times for $\max[\mathcal{K}(y,0)]/\min[\mathcal{K}(y,0)] = 12$, and reached an approximately constant value of 11 at long times for $\max[\mathcal{K}(y,0)]/\min[\mathcal{K}(y,0)] = 300$. Besides the importance of these results for fundamental reasons, these results also have important implications for the construction of models for the SFML. In particular, the strong non-Gaussianity of the velocity field in the SFML may be problematic since the vast majority of models (including the BHRZ model, as discussed in Sect. 3) for inhomogeneous turbulent flows make closure approximations that are only strictly justifiable in the limit where the PDF of $\boldsymbol{u}(\boldsymbol{x},t)$ is only weakly perturbed from a Gaussian.

3 BHRZ model for the SFML

We shall now introduce the BHRZ model and consider in detail the various assumptions that have been made in its construction. Such a detailed presentation of the model will prove to be useful when we come to compare its predictions with the DNS data for the SFML in Sect. 4. We then consider the specification of certain constants appearing in the model and then present the initial and boundary conditions used in the BHRZ model for the SFML. It is important to note that what we are here calling BHRZ actually differs in some respects to the original BHRZ model presented in Besnard et al. [6], in particular, the specification of the timescale of the turbulent scales of motion and the symmetrization of the physical-space transport term (both of these differences are discussed below). Nevertheless, we retain the name BHRZ since that is the origin of the essential modeling framework that we are considering here.

3.1 Formulation of the model

The BHRZ model begins by considering $\boldsymbol{\mathcal{R}}_2(\boldsymbol{x}_1,\boldsymbol{x}_2,t) \equiv \langle \boldsymbol{u}(\boldsymbol{x}_1,t)\boldsymbol{u}(\boldsymbol{x}_2,t)\rangle$, the two-point, one-time correlation tensor of the fluid velocity field $\boldsymbol{u}(\boldsymbol{x},t)$, for which an evolution equation can be obtained from the incompressible NSE. Applying the transformation $[\boldsymbol{x}_1,\boldsymbol{x}_2] \to [\boldsymbol{x}+\boldsymbol{r}/2, \boldsymbol{x}-\boldsymbol{r}/2]$ to the evolution equation for $\boldsymbol{\mathcal{R}}_2(\boldsymbol{x}_1,\boldsymbol{x}_2,t)$, and then applying a Fourier transform conjugate to $\boldsymbol{r}$, we obtain (for $\boldsymbol{\partial_x}\langle \boldsymbol{u}(\boldsymbol{x},t)\rangle = \boldsymbol{0}$)

$$\partial_t \boldsymbol{\mathcal{R}}_2(\boldsymbol{x},\boldsymbol{k},t) = \mathcal{V}\boldsymbol{\mathcal{R}}_2 + \boldsymbol{\mathcal{N}} + \boldsymbol{\mathcal{N}}^\dagger, \tag{8}$$

where '†' denotes the Hermitian,

$$\mathcal{V}(\boldsymbol{x},\boldsymbol{k}) \equiv -2\nu k^2 + (\nu/2)\partial_x^2, \tag{9}$$

$$\mathcal{N}_{ij}(\boldsymbol{x},\boldsymbol{k},t) \equiv -\nabla_n \mathcal{R}_{3,inj}(\boldsymbol{x},\boldsymbol{k},t) - \nabla_i \int_{\mathbb{R}^3} G(\boldsymbol{x},\boldsymbol{x}',\boldsymbol{k})\nabla'_m\nabla'_n \mathcal{R}_{3,mnj}(\boldsymbol{x}',\boldsymbol{k},t)\,d\boldsymbol{x}',$$

$$\begin{aligned}
\mathcal{R}_{2,ij}(\boldsymbol{x},\boldsymbol{k},t) &\equiv \int_{\mathbb{R}^3} e^{-i\boldsymbol{k}\cdot\boldsymbol{r}}\Big\langle u_i(\boldsymbol{x}+\boldsymbol{r}/2,t)u_j(\boldsymbol{x}-\boldsymbol{r}/2,t)\Big\rangle d\boldsymbol{r},\\
\mathcal{R}_{3,inj}(\boldsymbol{x},\boldsymbol{k},t) &\equiv \int_{\mathbb{R}^3} e^{-i\boldsymbol{k}\cdot\boldsymbol{r}}\Big\langle u_i(\boldsymbol{x}+\boldsymbol{r}/2,t)u_n(\boldsymbol{x}+\boldsymbol{r}/2,t)u_j(\boldsymbol{x}-\boldsymbol{r}/2,t)\Big\rangle d\boldsymbol{r},
\end{aligned} \tag{10}$$

$$\nabla_m \equiv \frac{1}{2}\frac{\partial}{\partial x_m} + ik_m,$$

and the Green function, $G(\boldsymbol{x}, \boldsymbol{x}', \boldsymbol{k})$, solves

$$-\nabla^2 G(\boldsymbol{x}, \boldsymbol{x}', \boldsymbol{k}) = \delta(\boldsymbol{x} - \boldsymbol{x}'), \quad \text{for } \boldsymbol{x} \in \mathbb{R}^3. \tag{11}$$

The term $\mathcal{V}\boldsymbol{\mathcal{R}}_2$ in (8) describes the contribution to the evolution of $\boldsymbol{\mathcal{R}}_2$ from molecular dissipation and diffusion, and is in closed form. The term $\boldsymbol{\mathcal{N}}$ is unclosed and contains contributions arising from two distinct terms in the NSE; the first coming from the nonlinear advection term, and the second from the pressure gradient term. The second contribution is non-local in physical space ($\boldsymbol{x}$-space) and makes the evolution equation for $\boldsymbol{\mathcal{R}}_2$ an integro-differential equation. The two contributions in $\boldsymbol{\mathcal{N}}$ collectively describe three physically distinct processes affecting the evolution of $\boldsymbol{\mathcal{R}}_2$; a redistribution effect, energy transport in $\boldsymbol{k}$-space and energy transport in $\boldsymbol{x}$-space. The BHRZ model closes $\boldsymbol{\mathcal{N}}$ phenomenologically, utilizing closures that qualitatively reproduce each of these physical processes.

The first step made in BHRZ is to integrate the evolution equation for $\boldsymbol{\mathcal{R}}_2(\boldsymbol{x}, \boldsymbol{k}, t)$ over spherical shells of constant $k \equiv \|\boldsymbol{k}\|$, defining

$$\boldsymbol{E}(\boldsymbol{x}, k, t) \equiv \int \boldsymbol{\mathcal{R}}_2(\boldsymbol{x}, \boldsymbol{k}, t) \frac{k^2}{(2\pi)^3} \, d\Omega_k, \tag{12}$$

such that

$$\mathcal{K}(\boldsymbol{x}, t) \equiv \int_0^\infty \mathrm{tr}[\boldsymbol{E}(\boldsymbol{x}, k, t)] \, dk, \tag{13}$$

is the TKE per unit mass at $(\boldsymbol{x}, t)$ and

$$\boldsymbol{R}_2(\boldsymbol{x}, t) \equiv \Big\langle \boldsymbol{u}(\boldsymbol{x}, t)\boldsymbol{u}(\boldsymbol{x}, t) \Big\rangle = 2 \int_0^\infty \boldsymbol{E}(\boldsymbol{x}, k, t) \, dk, \tag{14}$$

is the one-point Reynolds stress tensor. Note that here and throughout, $\boldsymbol{\mathcal{R}}_N$, is used to denote the N^{th} order velocity correlation tensors in $(\boldsymbol{x}, \boldsymbol{k}, t)$-space, whereas $\boldsymbol{R}_N$ is used to denote them in $(\boldsymbol{x}, t)$-space. Furthermore, when expressed using index notation, the components of these tensors are denoted by $\mathcal{R}_{N,\alpha_1,\ldots,\alpha_N}$ and $R_{N,\alpha_1,\ldots,\alpha_N}$, where $\alpha_1, \ldots, \alpha_N$ denote the N indices of the tensor.

As discussed in Besnard et al. [6], the integration over spherical shells ("angle averaging") is introduced merely to reduce the dimensionality of the solution space of the model. Such a procedure is without justification in the general case of anisotropic velocity fields and impacts the ability of the model to represent anisotropic dynamics in $\boldsymbol{k}$-space. The precise way in which this angle averaging affects the ability of the model to accurately predict the evolution of $\boldsymbol{\mathcal{R}}_2$ is not entirely understood. However, recent work has made a step toward understanding these effects by constructing tensor spherical harmonic expansions for objects such as $\boldsymbol{\mathcal{R}}_2$ (in homogeneous flows) that can be used to consider the evolution and contribution of the terms neglected through the spherical average to the evolution of $\boldsymbol{\mathcal{R}}_2$ (see Rubinstein et al. [18]). It should be noted, however, that this spherical averaging only directly suppresses the anisotropy description in $\boldsymbol{k}$-space, that is, in scale, and not $\boldsymbol{x}$-space, that is, in position. This is important because the transport of $\boldsymbol{\mathcal{R}}_2$ that dominates the mixing in the SFML and generates the flow field anisotropy is dominated by the motion of the largest scales of the flow, and this transport occurs in $\boldsymbol{x}$-space. Thus, much of the anisotropy of the flow that is important for the mixing process is still captured through the models description of anisotropy in $\boldsymbol{x}$-space.

With the spherical averaging operation applied to the evolution equation for $\boldsymbol{\mathcal{R}}_2$, we then have

$$\partial_t \boldsymbol{E}(\boldsymbol{x}, k, t) \equiv \mathcal{V}\boldsymbol{E} + \underbrace{\int \Big[\boldsymbol{\mathcal{N}}(\boldsymbol{x}, \boldsymbol{k}, t) + \boldsymbol{\mathcal{N}}^\dagger(\boldsymbol{x}, \boldsymbol{k}, t)\Big] \frac{k^2}{(2\pi)^3} \, d\Omega_k}_{\boldsymbol{N}(\boldsymbol{x},k,t)}, \tag{15}$$

and BHRZ introduce phenomenological closures to capture the distinct physical processes described by $\boldsymbol{N}$. In particular, they introduce $\boldsymbol{N} \approx \boldsymbol{\mathcal{A}} + \boldsymbol{\mathcal{T}}^k + \boldsymbol{\mathcal{T}}^y$, where the three terms describe the processes of redistribution, transport in k-space and transport in y-space. In the following, for simplicity, we only discuss the form of the BHRZ closures that are applicable to the SFML, for which the terms in the evolution equation for $\boldsymbol{\mathcal{R}}_2$ are described by the reduced variables $(y, k, t) \equiv (x_2, k, t)$.

The redistribution effect in $\boldsymbol{N}$ does not contribute to the evolution of $\mathcal{K}$, but instead redistributes the energy among the different components of the velocity field. For example, in a one-point equation for $\boldsymbol{R}_2$, the redistribution effect in a homogeneous turbulent velocity field is described by $\langle p(\boldsymbol{x}, t)\boldsymbol{\nabla}\boldsymbol{u}(\boldsymbol{x}, t)\rangle$, which does not

contribute to $\mathcal{K}(\boldsymbol{x},t)$ in an incompressible velocity field since $\mathrm{tr}[\langle p(\boldsymbol{x},t)\boldsymbol{\nabla}\boldsymbol{u}(\boldsymbol{x},t)\rangle] = \boldsymbol{0}$. It is common to assume, especially when constructing models, that the nature of the redistribution effect is to drive $\boldsymbol{u}(\boldsymbol{x},t)$ toward an isotropic state (though this need not be the case), and following this line of thought, BHRZ models the redistribution effect with a linear return-to-isotropy term

$$\boldsymbol{\mathcal{A}}(y,k,t) \equiv c_M \Phi\Big((E/3)\mathbf{I} - \boldsymbol{E}\Big), \tag{16}$$

where c_M is a dimensionless constant (the model constants introduced in this section are discussed in Sect. 3.2), and $E(y,k,t) \equiv \mathrm{tr}[\boldsymbol{E}(y,k,t)]$. The frequency $\Phi(y,k,t)$ (inverse eddy turnover timescale at scale k, and location y) is defined in [6] as $\Phi(y,k,t) \equiv \sqrt{k^3 E(y,k,t)}$. We instead choose the form for $\Phi(y,k,t)$ suggested in Rubinstein and Clark [19] that captures the viscous effects on the frequency (which we found to be important for describing the low Reynolds number SFML considered in Tordella et al. [16]), namely

$$\Phi(y,k,t) = (1/2)\Big[\Big(\nu^2 k^4 + 4H\Big)^{1/2} - \nu k^2\Big], \tag{17}$$

$$H(y,k,t) \equiv c_H \int_0^k q^2 E(y,q,t)\, dq, \tag{18}$$

where $c_H = 2/9$ (see Rubinstein and Clark [19]).

The closure in (16) represents the simplest model for the return-to-isotropy tensor and ignores contributions involving nonlinear combinations of the anisotropy measure $(E/3)\mathbf{I} - \boldsymbol{E}$. In the context of one-point turbulence models where the return-to-isotropy term is proportional to $(\mathrm{tr}[\boldsymbol{R}_2]/3)\mathbf{I} - \boldsymbol{R}_2$, such linear return-to-isotropy models are known to be qualitatively incorrect [20]. However, its use in BHRZ allows for a more faithful representation of the return-to-isotropy process since in this case the model is able to capture the fact that different scales of motion in the turbulence return-to-isotropy at different rates, according to the correlation timescale of their motion. Indeed, in Clark and Zemach [13], it was found that the BHRZ model was able to capture the evolution of the flow anisotropy quite well, for the case of a homogeneous sheared and strained turbulent flow.

The transport in k-space is modeled using an advection-diffusion equation of the form proposed by Leith [21]

$$\boldsymbol{\mathcal{T}}^k(y,k,t) \equiv -c_1 \partial_k\Big(k\Phi\boldsymbol{E}\Big) + c_2 \partial_k\Big(k^2\Phi\partial_k\boldsymbol{E}\Big), \tag{19}$$

where c_1 and c_2 are dimensionless constants. The use of such a model approximates the k-space transport as being local in k-space, and indeed in Clark et al. [22] it was shown that the structure of the Leith diffusion model can be understood to arise from restricting the triad interactions in renormalized perturbation theories of turbulence to local interactions. Such a local truncation is in principle inconsistent with the NSE that describes non-local interactions among the scales of the turbulent velocity field. However, there are rigorous theoretical and numerical results that support the idea that the energy transport among scales in the inertial range of homogeneous, isotropic turbulence is dominated by local scale interactions [23]. This at least suggests that in the limit of weak inhomogeneity, the BHRZ model for the k-space energy transport is reasonable. Comparisons of results from the BHRZ model to results from the non-local EDQNM model in Besnard et al. [6] showed close agreement, also suggesting that the non-local interactions play a small role.

The transport in $\boldsymbol{x}$-space is modeled in BHRZ in essentially two steps: First, a local approximation is made to the non-local (in $\boldsymbol{x}$-space) pressure-transport in $\boldsymbol{\mathcal{N}}$. This amounts to ignoring the $\boldsymbol{\partial}'_{\boldsymbol{x}}$ contribution to $\boldsymbol{\nabla}'$ in the integrand defining the pressure-velocity transport [see (10)], giving

$$\begin{aligned}
\mathcal{N}_{ij}(\boldsymbol{x},\boldsymbol{k},t) &= -\nabla_n \mathcal{R}_{3,inj}(\boldsymbol{x},\boldsymbol{k},t) - \nabla_i \int_{\mathbb{R}^3} G(\boldsymbol{x},\boldsymbol{x}',\boldsymbol{k})\nabla'_m \nabla'_n \mathcal{R}_{3,mnj}(\boldsymbol{x}',\boldsymbol{k},t)\, d\boldsymbol{x}' \\
&\approx -\nabla_n \mathcal{R}_{3,inj}(\boldsymbol{x},\boldsymbol{k},t) - \nabla_i \int_{\mathbb{R}^3} \delta(\boldsymbol{x}-\boldsymbol{x}')k^{-2}k_m k_n \mathcal{R}_{3,mnj}(\boldsymbol{x}',\boldsymbol{k},t)\, d\boldsymbol{x}' \\
&= -\nabla_n \mathcal{R}_{3,inj}(\boldsymbol{x},\boldsymbol{k},t) - k^{-2}k_m k_n \nabla_i \mathcal{R}_{3,mnj}(\boldsymbol{x},\boldsymbol{k},t).
\end{aligned} \tag{20}$$

This local approximation is introduced only for the purposes of simplification, to reduce the equation for $\partial_t \boldsymbol{\mathcal{R}}_2$ from an integro-differential equation to a PDE. However, the step is only (approximately) justified if

$\|\boldsymbol{k}\boldsymbol{\mathcal{R}}_{\boldsymbol{3}}\| \gg \|\boldsymbol{\partial}_{\boldsymbol{x}}\boldsymbol{\mathcal{R}}_{\boldsymbol{3}}\|$. This is satisfied either for a flow that is weakly inhomogeneous, or else if one is only interested in the high-wavenumbers of the velocity field. In the SFML, there is a strong inhomogeneity with turbulent mixing driven by the low wavenumbers of the velocity field. As such, the local pressure approximation may be problematic for the SFML and inhomogeneous turbulent flows in general.

The resulting $\boldsymbol{x}$-space transport terms described by $\boldsymbol{N} \equiv \int[\boldsymbol{\mathcal{N}}+\boldsymbol{\mathcal{N}}^{\dagger}]\frac{k^2}{(2\pi)^3}\,d\Omega_k$ contain (spherical integrals involving) $\boldsymbol{\mathcal{R}}_3$, and this is closed by using a gradient-diffusion approximation, wherein $\boldsymbol{\mathcal{R}}_3$ is related to the gradients of $\boldsymbol{\mathcal{R}}_2$, giving the spherically averaged result (in component form)

$$\mathcal{T}^{y}_{ij}(y,k,t) \equiv c_D\partial_y\Big(\mathscr{D}_{22}\partial_y E_{ij} + \mathscr{D}_{j2}\partial_y E_{2i} + \mathscr{D}_{i2}\partial_y E_{j2}\Big), \tag{21}$$

where c_D is a dimensionless constant and $\boldsymbol{\mathscr{D}}(y,t)$ is a diffusion tensor, defined as

$$\boldsymbol{\mathscr{D}}(y,t) \equiv \int_0^{\infty} \Phi^{-1}(y,q,t)\boldsymbol{E}(y,q,t)\,dq. \tag{22}$$

The form of the closure in (21) differs from that proposed in the original BHRZ model: In Besnard et al. [6] they discuss a closure of the form given in (21) but subsequently choose to adopt a simpler closure $\boldsymbol{\mathcal{T}}^{y} = c_D\partial_y(\nu_T\partial_y\boldsymbol{E})$. However, this simplified form does not correctly preserve the component coupling of $\boldsymbol{u}(\boldsymbol{x},t)$, and for the SFML with initially isotropic $\boldsymbol{E}$, the use of the simplified model for $\boldsymbol{\mathcal{T}}^{y}$ in BHRZ would lead to the incorrect prediction that $\boldsymbol{E}(y,k,t) \propto \mathbf{I}\,\forall t$.

For strongly inhomogeneous turbulent flows, the local approximation to the pressure-transport in $\boldsymbol{x}$-space is likely in significant error, since in such a flow, $\boldsymbol{\mathcal{R}}_3$ will vary considerably over the range of the support of the integrand describing the pressure-transport. According to the analysis in Aluie and Eyink [24], the locality of the $\boldsymbol{k}$-space energy transport essentially follows from the particular scaling properties of the Fourier transform of the velocity field, i.e. $\boldsymbol{u}(\boldsymbol{k},t)$, for $\boldsymbol{k}$ in the inertial range, and these scalings are to some degree universal. In contrast, the $\boldsymbol{x}$-space energy transport depends mainly upon the motion of the largest scales of the turbulence, whose scaling is fundamentally different to that of the velocity differences in the inertial range, and furthermore, their behavior is entirely problem dependent (i.e. definitely not universal). Therefore, whereas locality of the transport in $\boldsymbol{k}$-space may hold (even approximately) for $\boldsymbol{k}$ in the inertial range of an inhomogeneous turbulent flow in the limit $Re_\lambda \to \infty$, there is no corresponding reason why there should be locality of the pressure-transport in $\boldsymbol{x}$-space for an incompressible flow.

Concerning the gradient-diffusion closure employed for $\boldsymbol{\mathcal{R}}_3$, this is only strictly applicable in the limit of weak inhomogeneity, where the PDF of $\boldsymbol{u}(\boldsymbol{x},t)$ is only weakly perturbed from a Gaussian (noting that the PDF of $\boldsymbol{u}(\boldsymbol{x},t)$ is essentially Gaussian in homogeneous turbulence).

With these phenomenological closures, the BHRZ model for $\boldsymbol{E}(y,k,t)$ in the SFML is

$$\partial_t\boldsymbol{E}(y,k,t) = \mathcal{V}\boldsymbol{E} + \boldsymbol{N} \approx \mathcal{V}\boldsymbol{E} + \boldsymbol{\mathcal{A}} + \boldsymbol{\mathcal{T}}^{y} + \boldsymbol{\mathcal{T}}^{k}. \tag{23}$$

3.2 Model constants

The closure model for $\boldsymbol{\mathcal{N}}+\boldsymbol{\mathcal{N}}^{\dagger}$ in (23), expressed through the terms $\boldsymbol{\mathcal{A}}$, $\boldsymbol{\mathcal{T}}^{y}$ and $\boldsymbol{\mathcal{T}}^{k}$, contains the unspecified, dimensionless constants c_D, c_1, c_2 and c_M. All but c_D, the turbulent diffusion coefficient, can be specified by considering theoretical, asymptotic constraints on the model for $\boldsymbol{E}(y,k,t)$. In particular, the expected scaling of $\boldsymbol{E}(y,k,t)$ for k in the inertial range when $Re_\lambda \to \infty$, and the constraint that in the absence of transport in k-space, the k-space behavior must satisfy the equipartition spectrum $\boldsymbol{E}(y,k,t) \propto k^2$ (see Clark and Zemach [13] for more details on the use of these asymptotic constraints to determine c_1, c_2 and c_M). The turbulent diffusion coefficient c_D cannot be specified using such asymptotic constraints because it is related to the physical-space transport, and this is dominated by the large scales of the flow which are entirely problem dependent. The only way to specify c_D is to match it to known data, and the SFML is a particularly good test case for doing this since in the SFML the transport of energy in physical space is entirely generated by the turbulence itself.

It is worth mentioning that obtaining c_D in this way does not in any way guarantee that the BHRZ model will accurately predict how the physical-space energy transport will vary across the mixing layer. This follows since c_D does not control the functional behavior of $\boldsymbol{\mathcal{T}}^{y}$, it simply changes its magnitude.

For the SFML, there are several ways that we could obtain an estimate for c_D; however, we choose to obtain the value of c_D by determining the value that gives the best predictions from the BHRZ model when compared

to the DNS data for the evolution of the mixing layer width $\Delta(t) \equiv Y_{[1/4]} - Y_{[3/4]}$, where $\mathscr{E}(Y_{[1/4]}, t) = 1/4$, $\mathscr{E}(Y_{[3/4]}, t) = 3/4$ and

$$\mathscr{E}(y,t) \equiv \frac{\min[\mathcal{K}(y,t)] - \mathcal{K}(y,t)}{\min[\mathcal{K}(y,t)] - \max[\mathcal{K}(y,t)]}, \tag{24}$$

is a normalized energy function $\mathscr{E}(y,t) \in [0,1]$.

There are at least two reasons for choosing this approach to determine c_D: First, $\Delta(t)$ is a function of only one dimension (time), making it a much simpler candidate for determining c_D than say $\mathcal{K}$, which depends on both y and t. Second, in Tordella and Iovieno [25] they found that $\Delta(t)$ has quite a weak dependence on both Re_λ and $\max[\mathcal{K}(y,0)]/\min[\mathcal{K}(y,0)]$. Therefore, determining c_D using $\Delta(t)$ will give a value which should depend weakly upon the initial conditions of the mixing layer. We choose to determine c_D, as described above, for the case with the smallest $\max[\mathcal{K}(y,0)]/\min[\mathcal{K}(y,0)]$. The reasoning behind this is that the turbulent transport closure employed in the BHRZ model is only strictly applicable for the case where the PDF of $\boldsymbol{u}(\boldsymbol{x},t)$ is weakly perturbed from a Gaussian. Such a situation would be realized in the limit $\max[\mathcal{K}(y,0)]/\min[\mathcal{K}(y,0)] \to 1$, and it is therefore in this limit that the BHRZ closure model should be most appropriate. In Sect. 4 we will discuss the choice of c_D further and the value we obtain for the SFML.

3.3 Initial and boundary conditions

With $\langle \boldsymbol{u}(y,0)\boldsymbol{u}(y,0)\rangle$ specified in (4), we construct the initial condition $\boldsymbol{E}(\boldsymbol{x},k,0)$ (required in the BHRZ model) as

$$\boldsymbol{E}(y,k,0) = \frac{\mathcal{E}(k,0)}{2\mathcal{K}^{[1]}}\Big\langle \boldsymbol{u}(y,0)\boldsymbol{u}(y,0)\Big\rangle, \tag{25}$$

$\mathcal{E}(k,0)$ being the energy spectrum corresponding to the homogeneous field $\boldsymbol{u}^{[1]}(\boldsymbol{x},0)$. We use the same data for the initial energy spectrum $\mathcal{E}(k,0)$ as was used in for the initial condition for the DNS in Tordella et al. [16]. One difference is that in the DNS, $\mathcal{E}(k,0)$ is only prescribed for $k \in [1, k_{max}]$ whereas in the BHRZ model we want to solve for $\boldsymbol{E}(y,k,t)$ on the interval $k \in [k_{min}, k_{max}]$, where $k_{min} \ll 1$ (to ensure the validity of the boundary condition at k_{min}, discussed below) and k_{max} is the maximum wavenumber. In order to specify $\mathcal{E}(k,0)$ for $k < 1$ for the BHRZ model initial condition, we extrapolate the DNS data for $\mathcal{E}(k,0)$, ensuring that the infrared power-law scaling of the extrapolated data for $\mathcal{E}(k,0)$ for $k < 1$ is consistent with the scaling of the original DNS data for $\mathcal{E}(k,0)$ at $k = \mathcal{O}(1)$.

We match the initial Re_λ of the flow specified in the model (through the value specified for ν) with that of the DNS. From the data for $\mathcal{E}(k,0)$ we can compute u_0', the r.m.s. velocity of $\boldsymbol{u}^{[1]}(\boldsymbol{x},0)$ and then λ_f (longitudinal Taylor microscale) through the relation

$$\lambda_f = \sqrt{2u_0'u_0'/\Big\langle[\nabla_1 u_1^{[1]}(y,t)]^2\Big\rangle}.$$

We then calculate the appropriate value of ν to use in the BHRZ model through $\nu = u_0'\lambda_f/Re_\lambda$, and in Tordella et al. [16] the Taylor Reynolds number of $\boldsymbol{u}^{[1]}(\boldsymbol{x},0)$ is $Re_\lambda = 45$. Using the energy spectrum data from Tordella et al. [16], we have $\max[\mathcal{K}(y,0)] = 0.922$, $u_0' = \sqrt{(2/3)\max[\mathcal{K}(y,0)]} = 0.784$ which gives $\nu \approx 0.0017$, and we use this value when solving the BHRZ model.

In Tordella et al. [16], periodic boundary conditions were used for $\boldsymbol{u}(\boldsymbol{x},t)$, with period L in the y direction. Corresponding to this, we specify periodic boundary conditions in the y domain, namely $\boldsymbol{E}(y,k,t) = \boldsymbol{E}(y+L,k,t)$. The boundary conditions in k-space are specified as follows: We introduce the variable $z \equiv \log[k]$ and enforce that the numerical grid be uniform in z-space. For small k, $\boldsymbol{E}(y,k,t) = \boldsymbol{J}k^n \implies \boldsymbol{E}(y,z,t) = \boldsymbol{J}e^{zn}$, where $\boldsymbol{J}$ is some tensor function of y and t. Using a Taylor series, we obtain the boundary condition for dummy node $z_{min} - \delta z$ (where $z_{min} \equiv \log[k_{min}]$)

$$\begin{aligned}\boldsymbol{E}(y, z_{min} - \delta z, t) &= \boldsymbol{E}(y, z_{min}, t) - \delta z \partial_z \boldsymbol{E}(y, z_{min}, t) + \mathcal{O}(\delta z^2)\\ &= \boldsymbol{J}e^{z_{min}n} - n\delta z \boldsymbol{J}e^{z_{min}n} + \mathcal{O}(\delta z^2)\\ &= e^{-n\delta z}\boldsymbol{E}(y, z_{min}, t) + \mathcal{O}(\delta z^2),\end{aligned} \tag{26}$$

and we take $n = 2$, consistent with the behavior of the DNS data for $\mathcal{E}(k,0)$ at $k = \mathcal{O}(1)$.

The boundary condition for k_{max} is specified as follows: Assuming that at high-k, $\boldsymbol{E}(y,k,t) = k^{\xi}\widetilde{\boldsymbol{E}}_{min}$, where $\widetilde{\boldsymbol{E}}_{min} \equiv k_{min}^{-1}\boldsymbol{E}(y,k_{min},t)$, then in z-space we have $\boldsymbol{E}(y,z,t) = \widetilde{\boldsymbol{E}}_{min}e^{z\xi}$. From this we construct the boundary condition for dummy node $z_{max}+\delta z$ ($z_{max} \equiv \log[k_{max}]$), which in component form is

$$E_{ij}(y,z_{max}+\delta z,t) = E_{ij}^2(y,z_{max},t)\Big/E_{ij}(y,z_{max}-\delta z,t). \tag{27}$$

4 Results and discussion

We begin by considering the results for the mixing-layer width $\Delta(t)$, introduced in Sect. 3.2. In Sect. 3.2 we discussed that the BHRZ value for c_D would be chosen as that value which gives the best fit for the BHRZ solution for $\Delta(t)$ compared with the DNS data. In Fig. 2a we first compare the DNS data with the BHRZ prediction obtained with $c_D = 0$, in order to determine how much of a contribution the turbulent transport gives to $\Delta(t)$ compared with the molecular diffusion contribution. The results indicate that the turbulence transport is by far the most dominant contribution to the evolution of $\Delta(t)$, even at the relatively low Re_λ of the flow ($\approx$45 at $t=0$).

For the case with $\gamma = 1$ (weakest initial inhomogeneity for which we have DNS data), we determined the value $c_D = 0.0145$. From Fig. 2b it can be seen that this choice of c_D gives good agreement between BHRZ the DNS data at long times, both qualitatively and quantitatively. Although another value could have been chosen to give a good match at small times, this would have led to significant errors at large times. Furthermore, on physical grounds, it makes more sense to match the solutions at longer times since the turbulence inhomogeneity weakens with increasing time, and it is in the regime of weak inhomogeneity that the approximations invoked in the BHRZ are most justified.

The value of c_D that we obtain is quite different to the value obtained for one-point models, e.g. in Hanjalic and Launder [26] the turbulent transport coefficient has a value 0.11. However, there is no reason to expect c_D to coincide with that in one-point models since the diffusion tensor in one-point models, $\mathbf{D}(y,t)$, is often defined as $\mathbf{D}(y,t) \equiv (\mathcal{K}/\langle\epsilon\rangle)\boldsymbol{R}_2$ and this is not equal to the diffusion tensor $\mathscr{D}(y,t)$ in the BHRZ model.

The results in Fig. 2a reveal that for $t/\tau < 2$ the BHRZ predictions are in error, overpredicting $\Delta(t)$ compared with the DNS. There are at least three possible reasons why $\boldsymbol{\mathcal{T}}^y$ could lead to these errors: First, the local approximation to the intrinsically non-local pressure-transport, second, the gradient-diffusion approximation for $\boldsymbol{\mathcal{R}}_3$ and third, the neglect of certain transient effects present in the DNS but not present in the model described by $\boldsymbol{\mathcal{T}}^y$. Considering the first two, although these are surely sources of error in the model applied to SFML where the inhomogeneity is strong, it is difficult to say what the nature of the errors introduced by these approximations would be, i.e. whether they would lead to over or under predictions of the energy transport in y-space. However, of these two, the local approximation to the pressure-transport is likely the main source of error. The reason for this is that in the initial stage of the evolution of the SFML, the PDF of $\boldsymbol{u}(\boldsymbol{x},t)$ is only slightly perturbed from its initial Gaussian form, and in that case the gradient-diffusion approximation for $\boldsymbol{\mathcal{R}}_3$ should be quite accurate. In contrast, the local approximation to the pressure-transport will be in greatest error during the initial stage of the evolution of the SFML since the inhomogeneity of the flow weakens with increasing t. Regarding the third reason, since the initial field in the DNS is constructed from weighted contributions of the homogeneous, isotropic velocity fields $\boldsymbol{u}^{[1]}(\boldsymbol{x},0)$ and $\boldsymbol{u}^{[2]}(\boldsymbol{x},0)$, the initial velocity field in the SFML satisfies $\langle\boldsymbol{u}(y,0)\boldsymbol{u}(y,0)\boldsymbol{u}(y,0)\rangle = \boldsymbol{0}$. Consequently, in the DNS, at $t=0$ there is no transport of energy in physical space. However, in the BHRZ model, $\boldsymbol{\mathcal{T}}^y(y,k,0) \neq \boldsymbol{0}$, which would lead to an overprediction of the initial growth of $\Delta(t)$. To examine whether or not this is the cause of the discrepancy observed in Fig. 2a, we performed the following test case. We used the DNS data at $t/\tau = 1$ as the 'initial condition' for the BHRZ model and then ran the model. In this case, at the 'initial time' $t/\tau = 1$, both the DNS and BHRZ model have a velocity field with finite energy transport in physical space. The results showed little difference,[1] suggesting that the overpredictions in Fig. 2a for $t/\tau < 2$ are in fact caused by either the local approximation to the pressure-transport or by the gradient-diffusion model for $\boldsymbol{\mathcal{R}}_3$.

We now consider the BHRZ predictions and DNS data for $\mathscr{E}(y,t)$, the normalized energy function (defined in (24)), which, unlike $\Delta(t)$, not only gives a measure of the mixing with time, but also how the energy behaves

[1] This test case also rules out another possible cause of the discrepancies: In the DNS, the initial velocity field is somewhat 'artificial' and it will take some time before the velocity field generated in the SFML becomes a true Navier–Stokes solution, with the correct coupling between the scales of motion etc. We would expect that this transition to the true Navier–Stokes dynamics takes $\mathcal{O}(\tau)$ to occur. Since the test case used $t/\tau = 1$, as the 'initial condition', the fact that the results showed little difference with those obtained using the true initial condition, $t/\tau = 0$, suggest that the effect of the artificiality of the initial condition in the DNS is only playing a minor role for the physical mechanisms governing the mixing in the velocity field.

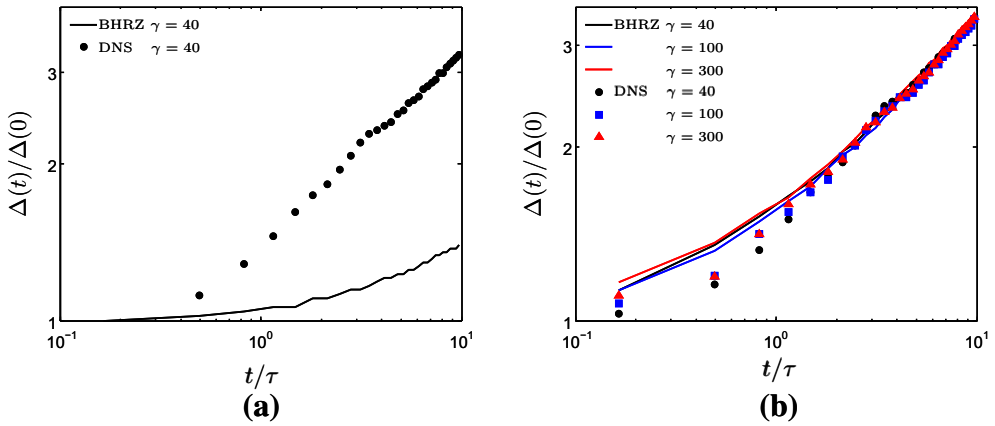

Fig. 2 Plot of BHRZ predictions and DNS data for $\Delta(t)/\Delta(0)$ with **a** $c_D = 0$ and (b) $c_D = 0.0145$. *Black line/symbols* are for $\gamma = 40$, *blue line/symbols* are for $\gamma = 100$ and *red line/symbols* are for $\gamma = 300$ (color figure online)

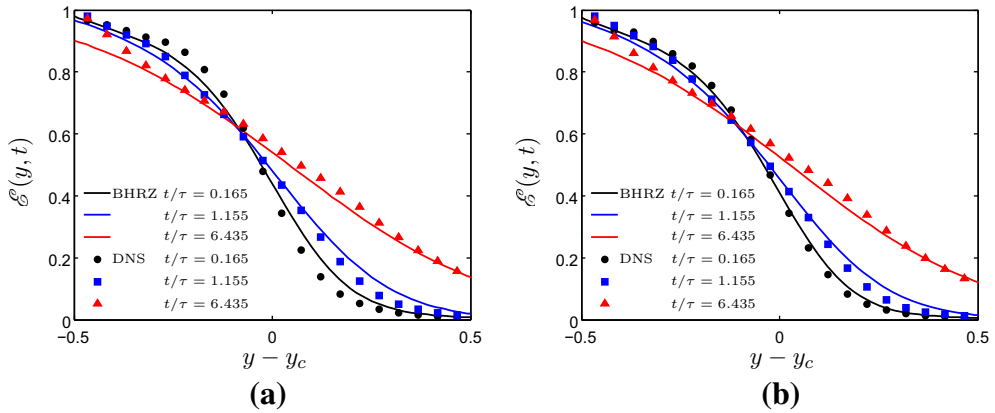

Fig. 3 Plot of BHRZ predictions (*lines*) and DNS data (*symbols*) for $\mathscr{E}(y,t)$ as a function of $y - y_c$ (where $y_c = L/2$) for **a** $\gamma = 40$ and **b** $\gamma = 300$. *Black symbols/line* correspond to $t/\tau = 0.165$, *blue symbols/line* to $t/\tau = 1.155$ and *red symbols/line* to $t/\tau = 6.435$ (color figure online)

as a function of position. The results in Fig. 3 show that the BHRZ model is able to predict $\mathscr{E}(y,t)$ quite well, capturing dependence on y.[2] That the BHRZ model predicts the dependence of $\mathscr{E}(y,t)$ on y as well as it does is somewhat surprising given that the transport model described by $\mathcal{T}^y$ is only strictly appropriate in the limit where the PDF of $\boldsymbol{u}(\boldsymbol{x},t)$ is weakly perturbed from a Gaussian; the results in Tordella et al. [16] show that even for $\gamma = 40$, the PDF of $\boldsymbol{u}(\boldsymbol{x},t)$ is quite far from being Gaussian. This suggests one of two things: First, it could simply suggest that the contributions from higher-order cumulants of the field $\boldsymbol{u}(\boldsymbol{x},t)$ to the physical-space transport are small. Second, it could imply that the contributions from higher-order cumulants of the field $\boldsymbol{u}(\boldsymbol{x},t)$ to the physical-space transport generate a similar dependance on y across the mixing layer (such that their effect is subsumed in the value determined for c_D).

Next, we compare the BHRZ predictions and the DNS data for the evolution of the turbulent kinetic energy $\mathcal{K}(y,t)/\mathcal{K}(y,0)$. In an inhomogeneous turbulent velocity field, there are essentially two ways that $\mathcal{K}(y,t)/\mathcal{K}(y,0)$ can change; through transport of energy to/away from y, and through viscous dissipation. For $y - y_c > 0$, $\mathcal{K}(y,t)/\mathcal{K}(y,0)$ may behave non-monotonically since these regions are receiving energy from the high energy side of the mixing layer, which could cause $\mathcal{K}(y,t)/\mathcal{K}(y,0)$ to increase, whereas viscous dissipation effects cause $\mathcal{K}(y,t)/\mathcal{K}(y,0)$ to decrease. The results in Fig. 4 confirm this non-monotonic behavior for $y - y_c > 0$, both in the DNS and the BHRZ model. The BHRZ results are in reasonable agreement with the DNS, though with a consistent underprediction in the long time regime. It is difficult to isolate a particular cause of these underpredictions since there are so many different effects in the system. One possibility is related to Φ, which is based upon a dimensional estimate for the turbulence time scales and may be therefore

[2] See Appendix for an explanation for the discrepancies at $y - y_c \lesssim -0.4$ for $t/\tau = 6.435$.

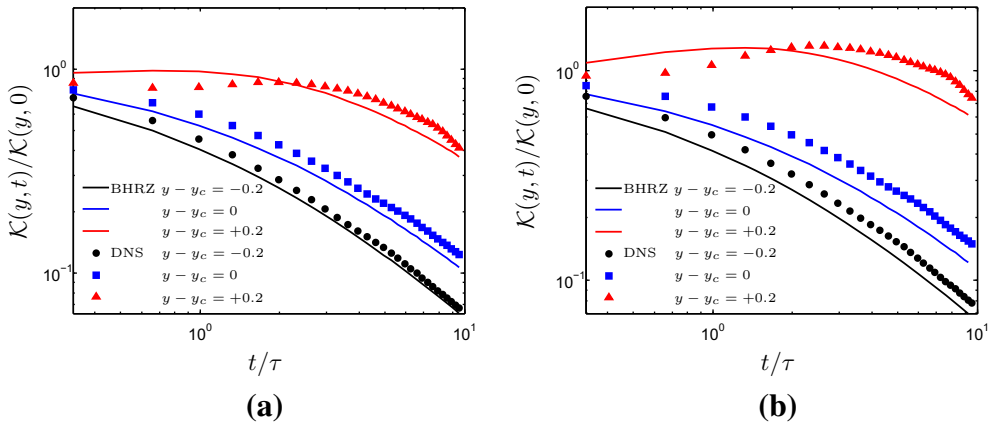

Fig. 4 Plot of BHRZ predictions and DNS data for $\mathcal{K}(y,t)/\mathcal{K}(y,0)$ at various y for **a** $\gamma = 40$ and **b** $\gamma = 300$. *Black symbols/line* correspond to $y - y_c = -0.2$, *blue symbols/line* to $y - y_c = 0$ and *red symbols/line* to $y - y_c = +0.2$ (color figure online)

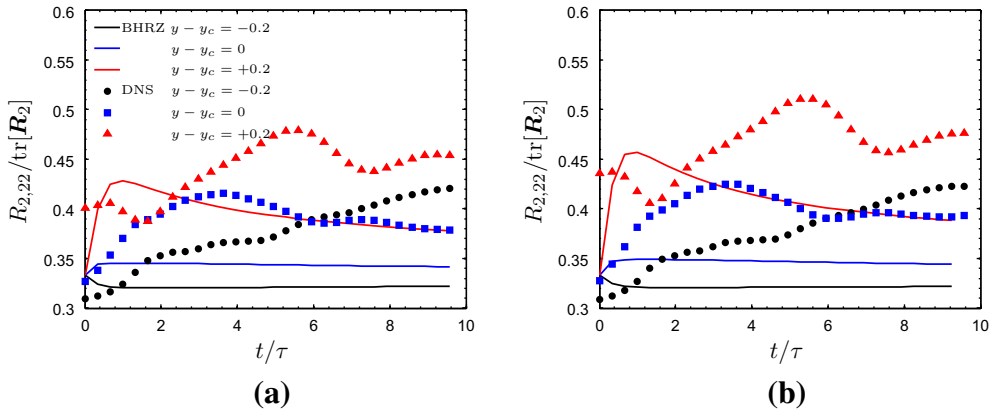

Fig. 5 Plot of BHRZ predictions and DNS data for $R_{2,22}/\mathrm{tr}[\boldsymbol{R}_2]$ at various $y - y_c$ for **a** $\gamma = 40$ and **b** $\gamma = 300$. *Black symbols/line* correspond to $y - y_c = -0.2$, *blue symbols/line* to $y - y_c = 0$ and *red symbols/line* to $y - y_c = +0.2$. Plot **b** legend corresponds to that in plot **a** (color figure online)

in error (relative to the 'true' timescale) by some $\mathcal{O}(1)$ factor. In particular, whereas the mixing is dominated by the largest flow scales, the dissipation is dominated by the smallest scales, but in the BHRZ model, the rate at which the energy is transferred from the large to the small scales is dependent upon Φ. Figure 4 also shows that the BHRZ model gives a reasonably good match with the DNS data for the decay exponent of the turbulent kinetic energy at long times.

Having considered the BHRZ results for the behavior of the turbulent kinetic energy during the mixing process, we now consider the behavior of the particular components of $\boldsymbol{R}_2(y,t)$. Comparing the components of this tensor reveal the evolution of the velocity field anisotropy during the mixing process. In Tordella et al. [16] it was observed that the velocity field evolved from its initially isotropic state to a self-similar anisotropic state for $t/\tau \gtrsim 2$, during which the anisotropy measure $R_{2,22}/\mathrm{tr}[\boldsymbol{R}_2]$ remained approximately constant.

Figure 5 shows a comparison of the BHRZ predictions and DNS data for the anisotropy measure $R_{2,22}/\mathrm{tr}[\boldsymbol{R}_2]$. The results reveal that the BHRZ model is in significant error in describing the evolution of the flow field anisotropy, and in particular, it significantly under-predicts the anisotropy when the SFML is in its self-similar regime. Within the BHRZ modeling framework, the anisotropy is generated exclusively by $\boldsymbol{\mathcal{T}}^y$, and the term $\boldsymbol{\mathcal{A}}$ drives the system back toward isotropy. The underpredictions could therefore be because $\boldsymbol{\mathcal{T}}^y$ is too small or else because $\boldsymbol{\mathcal{A}}$ is too large. To consider this, in Fig. 6 we show results where we compare the BHRZ predictions using the original value of c_M and also using $c_M = 0$ (corresponding to $\boldsymbol{\mathcal{A}} = \boldsymbol{0}$).

The results reveal that for the BHRZ model, $\boldsymbol{\mathcal{A}}$ is playing a small role and that the behavior of $R_{2,22}/\mathrm{tr}[\boldsymbol{R}_2]$ predicted by BHRZ is almost entirely controlled by $\boldsymbol{\mathcal{T}}^y$. As discussed earlier, these errors are either associated with the angle averaging operation applied to the transport equation, the local approximation to the pressure-

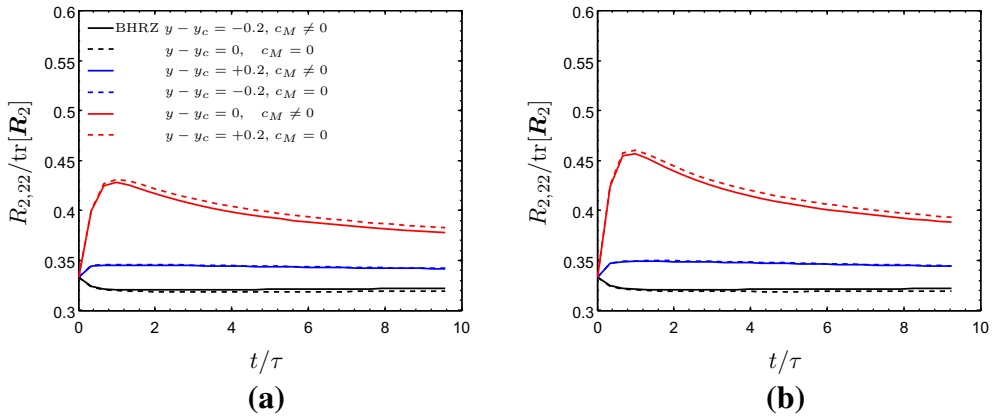

Fig. 6 Plot of BHRZ predictions and DNS data for $R_{2,22}/\mathrm{tr}[\boldsymbol{R}_2]$ at various $y - y_c$ for **a** $\gamma = 40$ and **b** $\gamma = 300$. *Black lines* correspond to $y - y_c = -0.2$, *blue lines* to $y - y_c = 0$ and *red lines* to $y - y_c = +0.2$. *Solid lines* are the results using the original BHRZ value for c_M, while the *dashed lines* are the results using $c_M = 0$. Plot **b** legend corresponds to that in plot **a** (color figure online)

transport or else the gradient-diffusion closure for $\boldsymbol{\mathcal{R}}_3$. Although it is difficult to estimate the effect of the first two approximations, we can obtain an estimate of the accuracy of the latter approximation.

The physical-space transport of $\boldsymbol{R}_2$ arising from the nonlinear advection and pressure gradient terms in the NSE is given by $\mathscr{F}(\boldsymbol{x}, t) \equiv -\boldsymbol{\partial_x} \cdot \langle \boldsymbol{uuu} \rangle - \boldsymbol{\partial_x} \langle p\boldsymbol{u} \rangle$. Applying to this the local approximation to the pressure field $p(\boldsymbol{x}, t)$ that was used in the construction of the BHRZ model we have

$$\mathscr{F}_{ij}(y, t) \approx \alpha \partial_y \langle u_i u_j u_2 \rangle \equiv \alpha \partial_y R_{3,ij2}, \tag{28}$$

where α is a coefficient that determines the contributions of the self-transport and (localized) pressure-transport to the overall transport $\mathscr{F}$. The BHRZ model for (28) is given by

$$\alpha \partial_y R_{3,ij2} \approx \int_0^\infty \mathcal{T}_{ij}^y(y, k, t)\, dk = \frac{c_D}{2} \partial_y \Big(\mathscr{D}_{22} \partial_y R_{2,ij} + \mathscr{D}_{j2} \partial_y R_{2,2i} + \mathscr{D}_{i2} \partial_y R_{2,j2} \Big). \tag{29}$$

For the SFML with $\boldsymbol{R}_2(y, 0) \propto \mathbf{I}$, $\boldsymbol{\mathcal{T}}^y(y, k, t)$ is diagonal $\forall t$, and using (29) with the definition of $\boldsymbol{\mathcal{T}}^y(y, k, t)$, this leads to the result

$$R_{3,ij2} \approx \frac{c_D}{2\alpha} \Big(2\delta_{2i}\delta_{2j} + 1 \Big) \mathscr{D}_{22} \partial_y R_{2,ij}, \tag{30}$$

(index summation is not implied) where we have used the condition that in the homogeneous regions of the SFML, $\boldsymbol{R}_3 = \mathbf{0}$ and $\partial_y \boldsymbol{R}_2 = \mathbf{0}$. In Fig. 7 we compare results from the DNS data for $R_{3,222}/(R_{3,112} + R_{3,222} + R_{3,332})$ with the corresponding predictions following from (30), that is

$$\frac{R_{3,222}}{R_{3,112} + R_{3,222} + R_{3,332}} \approx \frac{3\partial_y R_{2,22}}{\partial_y R_{2,11} + 3\partial_y R_{2,22} + \partial_y R_{2,33}}, \tag{31}$$

where we evaluate $\partial_y \boldsymbol{R}_2(y, t)$ using the DNS data. Although the data are quite noisy, the results in Fig. 7 seem to show that the gradient-diffusion closure gives quite a good approximation for the anisotropy of $\boldsymbol{R}_3(y, t)$. Certainly, the relative differences between the predictions of (31) and the DNS data are insufficient to explain the much larger relative differences between the BHRZ predictions and the DNS data for the anisotropy of $\boldsymbol{R}_2(y, t)$ observed in Fig. 5. This then indicates that the main source of error in the BHRZ prediction for $R_{2,22}/\mathrm{tr}[\boldsymbol{R}_2]$ arises from either the angle averaging operation applied to the evolution equation or else the local approximation for the pressure-transport.[3]

[3] There is in fact another possible cause for the discrepancies in the anisotropy results: Recall that in the DNS, the statistics are constructed by averaging over the homogeneous directions, for a given y, t. This leaves open the possibility that certain 'phase' information remains in the statistics, that would otherwise be averaged out, or at least suppressed, under a true ensemble average (average over infinitely many flow fields for a given y, t), and this could affect the anisotropy results. However, we do not know how significant these phase effects are, whereas it is possible to show from the transport equations that the angle averaging operation and the local approximation for the pressure-transport will certainly affect the anisotropy predicted by BHRZ.

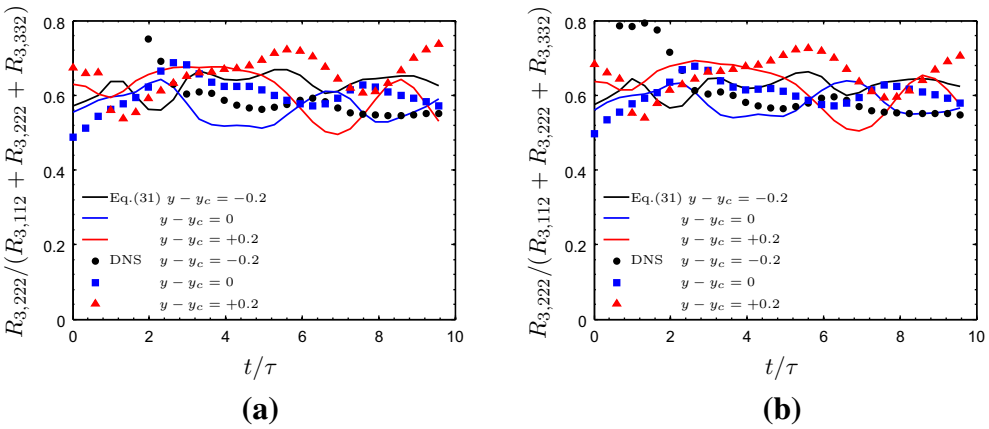

Fig. 7 Plot of predictions from (31) and DNS data for $R_{3,222}/(R_{3,112}+R_{3,222}+R_{3,332})$ at various $y-y_c$ for **a** $\gamma=40$ and **b** $\gamma=300$. *Black symbols/line* correspond to $y-y_c=-0.2$, *blue symbols/line* to $y-y_c=0$ and *red symbols/line* to $y-y_c=+0.2$ (color figure online)

The way in which the local approximation can affect the anisotropy predicted by BHRZ can be understood as follows. In the BHRZ framework, the difference between the true and the localized form of the pressure-transport contribution to $\boldsymbol{\mathcal{N}}$, $\Delta\boldsymbol{\mathcal{P}}$, is given by

$$\Delta\mathcal{P}_{ij} \equiv -\nabla_i \int_{\mathbb{R}^3} \Big(G(\boldsymbol{x},\boldsymbol{x}',\boldsymbol{k})\nabla'_m\nabla'_n - \delta(\boldsymbol{x}-\boldsymbol{x}')k^{-2}k_m k_n \Big)\mathcal{R}_{3,mnj}(\boldsymbol{x}',\boldsymbol{k},t)\,d\boldsymbol{x}', \tag{32}$$

which represents the error introduced into the BHRZ model of the pressure-transport description because of the local approximation. Since in an anisotropic flow we would in general expect that $\mathcal{R}_{3,mn1} \neq \mathcal{R}_{3,mn2} \neq \mathcal{R}_{3,mn3}$ (and also for their gradients), then (32) shows that the error introduced to $\boldsymbol{\mathcal{R}}_2$ (and hence $\boldsymbol{R}_2$) by the local approximation will differ for different components of $\boldsymbol{\mathcal{R}}_2$. It is in this way that the local approximation to the pressure-transport will affect the ability of the model to predict the anisotropy of the fluid velocity field.

Exactly how the angle averaging and local pressure-transport approximations affect the BHRZ prediction for the generation of the flow anisotropy are, however, difficult to determine (for example we do not know the behavior of $\boldsymbol{\mathcal{R}}_3$ in the SFML), and a detailed investigation of these effects will be addressed in future work.

5 Conclusion

In this paper we have presented a comparison of the BHRZ spectral model for inhomogeneous turbulence with DNS data of a Shear-Free Mixing Layer (SFML). One of the reasons for choosing this flow is that it provides us with the opportunity to scrutinize the BHRZ model for the physical-space transport of the turbulent velocity field. We found that the model is able to capture certain features of the SFML quite well for intermediate to long times, including the evolution of the mixing-layer width and turbulent kinetic energy. At short-times, and for more sensitive statistics such as the generation of the velocity field anisotropy, the model is less accurate. We have presented arguments that the main causes of the discrepancies are the angle averaging operations applied to the transport equations and the local approximation to the intrinsically non-local pressure-transport in physical space that was made in the BHRZ model. Recent work [18] provides a way to assess the effects of the angle averaging operation on the model prediction of the flow field anisotropy, and this is work underway. An important next step is to incorporate non-local transport into the BHRZ model to overcome the deficiencies arising from the local approximation.

Acknowledgements The authors would like to thank Daniela Tordella and Michele Lovieno for kindly providing us with the data from their paper Tordella et al., Phys. Rev. E, vol. 77, 016309, 2008. We would also like to thank Robert Rubinstein for reading through the paper and providing helpful feedback, and an anonymous referee for point out an issue regarding the initial condition used in the SFML that we had previously overlooked. ADB and SK acknowledge support from the Mix and Burn project, ASC Physics and Engineering Models Program. Work at the Los Alamos National Laboratory, through the ASC Program, was performed under the auspices of the U.S. DOE Contract No. DE-AC52-06NA25396. TTC was supported by a Los Alamos National Laboratory subcontract to the University of New Mexico, No. 325696.

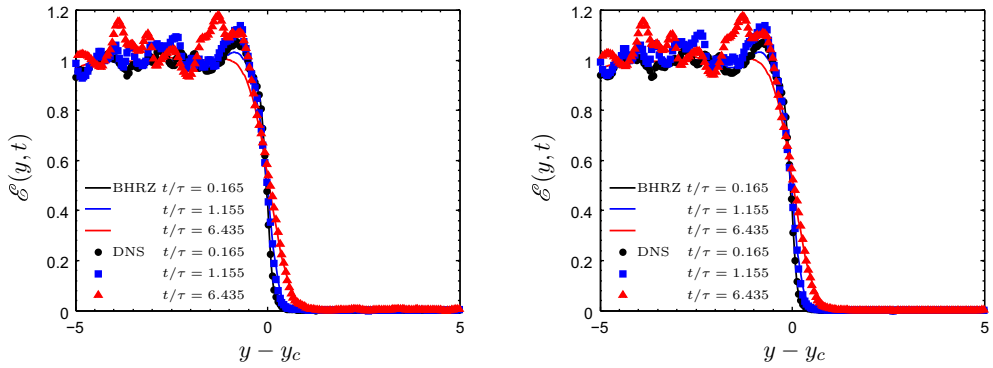

Fig. 8 Plot of BHRZ predictions and DNS data for $\mathscr{E}(y,t)$ as a function of $y - y_c$ (where $y_c = L/2$) for **a** $\gamma = 40$ and **b** $\gamma = 300$. *Black symbols/line* correspond to $t/\tau = 0.165$, *red symbols/line* to $t/\tau = 1.155$ and *blue symbols/line* to $t/\tau = 6.435$ (color figure online)

Appendix

In this appendix we discuss the discrepancies noted in Fig. 3 between the BHRZ predictions and the DNS data for $y - y_c \lesssim -0.4$.

In plotting the DNS data for the function $\mathscr{E}(y,t)$ we must determine $\max[\mathcal{K}(y,t)]$. However, as can be seen from Fig. 8, the data are noisy for $y - y_c \lesssim -0.4$ making it difficult to determine $\max[\mathcal{K}(y,t)]$. We therefore decided to choose $\max[\mathcal{K}(y,t)]$ as the value about which the data approximately oscillates at $y - y_c \leq -3$. This leads to an apparent underprediction of the BHRZ model for $\mathscr{E}(y,t)$ in the regime $-1 \lesssim y - y_c \lesssim -0.4$, as seen in Fig. 8. It seems clear that this is actually a consequence of the noise in the data in this regime, rather than a genuine underprediction of the BHRZ model since the DNS results in Ireland and Collins [27], which are also for a SFML, do not exhibit such noise and show data for $\mathcal{K}(y,t)$ (and hence $\mathscr{E}(y,t)$) that monotonically decreases with increasing y for $t \geq 0$.

References

1. Pope, S.B.: Turbulent Flows. Cambridge University Press, New York (2000)
2. Cadiou, A., Hanjalić, K., Stawiarski, K.: A two-scale second-moment turbulence closure based on weighted spectrum integration. Theor. Comput. Fluid Dyn. **18**(1), 1–26 (2004)
3. Schiestel, R.: Multiple-timescale modeling of turbulent flows in one-point closures. Phys. Fluids **30**(3), 722–731 (1987)
4. Clark, T.T., Zemach, C.: Symmetries and the approach to statistical equilibrium in isotropic turbulence. Phys. Fluids **10**, 2846–2858 (1998)
5. Clark, T.T.: Modeling Complex Turbulent Flows. chapter Two-Point Closures and Statistical Equilibrium. Springer Netherlands, Dordrecht (1999)
6. Besnard, D.C., Harlow, F.H., Rauenzahn, R.M., Zemach, C.: Spectral transport model for turbulence. Theor. Comput. Fluid Dyn. **8**, 1–35 (1996)
7. Kraichnan, R.H.: The structure of isotropic turbulence at very high Reynolds numbers. J. Fluid Mech. **5**, 497–543 (1959)
8. Wyld, H.W., Jr.: Formulation of the theory of turbulence in an incompressible fluid. Ann. Phys. **14**, 143–165 (1961)
9. Martin, P.C., Siggia, E.D., Rose, H.A.: Statistical dynamics of classical systems. Phys. Rev. A **8**, 423–437 (1973)
10. McComb, W.D.: A local energy-transfer theory of isotropic turbulence. J. Phys. A Math. Nucl. Gen. **7**(5), 632 (1974)
11. Daly, B., Harlow, F.H.: Transport equations in turbulence. Phys. Fluids **13**, 2634 (1970)
12. Launder, B.E., Reece, G.J., Rodi, W.: Progress in the developments of a Reynolds stress turbulent closure. J. Fluid Mech. **68**, 537–566 (1975)
13. Clark, T.T., Zemach, C.: A spectral model applied to homogeneous turbulence. Phys. Fluids A **7**, 1674 (1995)
14. Veeravalli, S., Warhaft, Z.: The shearless turbulence mixing layer. J. Fluid Mech. **207**, 191–229 (1989)
15. Thormann, A., Meneveau, C.: Decaying turbulence in the presence of a shearless uniform kinetic energy gradient. J. Turbul. **16**(5), 442–459 (2015)
16. Tordella, D., Iovieno, M., Bailey, P.R.: Sufficient condition for Gaussian departure in turbulence. Phys. Rev. E **77**, 016309 (2008)
17. Gilbert, B.: Diffusion mixing in grid turbulence without mean shear. J. Fluid Mech. **100**(2), 349–365 (1980)
18. Rubinstein, R., Kurien, S., Cambon, C.: Scalar and tensor spherical harmonics expansion of the velocity correlation in homogeneous anisotropic turbulence. J. Turbul. **16**(11), 1058–1075 (2015)
19. Rubinstein, R., Clark, T.T.: A generalized heisenberg model for turbulent spectral dynamics. Theor. Comput. Fluid Dyn. **17**, 249–272 (2004)

20. Lumley, J.L., Newman, G.R.: Return to isotropy of homogeneous turbulence. J. Fluid Mech. **82**, 161–178 (1977)
21. Leith, C.E.: Diffusion approximation to inertial energy transfer in isotropic turbulence. Phys. Fluids **10**, 1409 (1967)
22. Clark, T.T., Rubinstein, R., Weinstock, J.: Reassessment of the classical turbulence closures: the Leith diffusion model. J. Turbul. **10**, N35 (2009)
23. Eyink, G.L., Aluie, H.: Localness of energy cascade in hydrodynamic turbulence. I. Smooth coarse graining. Phys. Fluids **21**(11), 115107 (2009)
24. Aluie, H., Eyink, G.L.: Localness of energy cascade in hydrodynamic turbulence. II. sharp spectral filter. Physics of Fluids **21**(11), 115108 (2009)
25. Tordella, D., Iovieno, M.: Small-scale anisotropy in turbulent shearless mixing. Phys. Rev. Lett. **107**, 194501 (2011)
26. Hanjalic, K., Launder, B.E.: A Reynolds stress model of turbulence and its application to thin shear flows. J. Fluid Mech. **52**, 609 (1972)
27. Ireland, P.J., Collins, L.R.: Direct numerical simulation of inertial particle entrainment in a shearless mixing layer. J. Fluid Mech. **704**(8), 301–332 (2012)